



# On the benefit of the negative-spherical-aberration imaging technique for quantitative HRTEM

C.L. Jia\*, L. Houben, A. Thust, J. Barthel

*Institute of Solid State Research and Ernst Ruska Centre for Microscopy and Spectroscopy with Electrons, Research Centre Jülich, D-52425 Jülich, Germany*

## ARTICLE INFO

Dedicated to Professor Hannes Lichte on the occasion of his 65th birthday.

### Keywords:

Aberration-corrected high-resolution transmission electron microscopy  
Negative  $C_s$  imaging  
Measurement precision

## ABSTRACT

Employing an aberration corrector in a high-resolution transmission electron microscope, the spherical aberration  $C_s$  can be tuned to negative values, resulting in a novel imaging technique, which is called the negative  $C_s$  imaging (NCSI) technique. The image contrast obtained with the NCSI technique is compared quantitatively with the image contrast formed with the traditional positive  $C_s$  imaging (PCSI) technique. For the case of thin objects negative  $C_s$  images are superior to positive  $C_s$  images concerning the magnitude of the obtained contrast, which is due to constructive rather than destructive superposition of fundamental contrast contributions. As a consequence, the image signal obtained with a negative spherical aberration is significantly more robust against noise caused by amorphous surface layers, resulting in a measurement precision of atomic positions which is by a factor of 2–3 better at an identical noise level. The quantitative comparison of the two alternative  $C_s$ -corrected imaging modes shows that the NCSI mode yields significantly more precise results in quantitative high-resolution transmission electron microscopy of thin objects than the traditional PCSI mode.

© 2009 Elsevier B.V. All rights reserved.

## 1. Introduction

The availability of spherical aberration ( $C_s$ ) correction has opened up a large field of applied materials research for high-resolution transmission electron microscopy (HRTEM). The first application of  $C_s$ -corrected electron microscopy aimed at the minimization of previously unavoidable contrast delocalization artefacts by employing a  $C_s$  value close to zero [1]. In a further step, optimum imaging conditions were derived based on the tunability of the spherical aberration, which provide minimum contrast delocalization and maximum phase contrast at the same time [2]. Under such optimized conditions the point resolution is extended up to the information limit of the instrument. A third decisive step on the way to modern aberration-corrected electron microscopy was the finding that an unusually high image contrast is obtained when employing a negative value of the spherical aberration in conjunction with an overfocus [3]. The related negative  $C_s$  imaging (NCSI) mode yields a negative phase contrast of atomic objects, with atomic columns appearing bright against a darker background. For thin objects, the novel NCSI mode leads to a substantially higher contrast compared to the dark atom images formed under the traditional positive  $C_s$  imaging (PCSI) mode (positive phase contrast). The origin of the enhanced contrast obtained with thin objects is a constructive superposition of linear and non-linear contributions to the total image contrast [4–6].

The enhanced contrast of negative  $C_s$  images has already been exploited in several studies of weakly scattering atoms surrounded by strongly scattering atoms in compound materials, such as oxygen in oxides [3,4,7]. The extraordinary results produced by the NCSI technique have recently been reviewed [6]. Due to the enhanced contrast, negative  $C_s$  images provide an excellent basis for quantitative measurements of various local structure properties at lattice defects such as grain boundaries, domain walls, interfaces, and dislocations in electroceramic materials [7–10]. In contrast to previous studies without  $C_s$  correction it is now possible to resolve individual atom columns, to measure their position with a precision down to a few picometers, and to determine the occupancy of the individual columns.

For quantitative HRTEM it is mandatory to have, on the one hand, an adequate resolution available in order to separate closely spaced atom columns, and to obtain on the other hand a sufficiently strong signal from these columns in order to achieve a high precision in model based maximum-likelihood methods for the quantification of the related position information [11–14]. Important conclusions on the selection of the appropriate imaging conditions for quantitative HRTEM can therefore be drawn from a quantitative comparison of the NCSI and the PCSI modes with respect to the obtained contrast and with respect to the resulting measurement precision of atomic column positions.

In the present study we report on the benefit of the NCSI mode for quantitative HRTEM by a direct comparison with the traditional PCSI mode. The aim of this work is to investigate quantitatively the difference between the two imaging modes by means of image calculations. First we investigate the influence of

\* Corresponding author.

E-mail address: [c.jia@fz-juelich.de](mailto:c.jia@fz-juelich.de) (C.L. Jia).

the two alternative imaging modes on the strength of the obtained image contrast. Second we quantify the precision obtained for the measurement of atom column positions including the effect of image noise caused by amorphous surface layers. Considering the technological relevance of perovskite materials, which exhibit important properties required by modern electronics, we select  $\text{SrTiO}_3$  as an exemplary reference material for the image calculations.

## 2. Image calculations

$\text{SrTiO}_3$  has a cubic perovskite structure with a lattice parameter  $a=0.3905$  nm. Fig. 1a shows a perspective view of a unit cell. Fig. 1b displays the projection of the structure along the  $[110]$  crystal direction. In this viewing direction three types of atomic columns are distinct, namely SrO, Ti, and O. All images were calculated with the electron beam parallel to the  $[110]$  zone axis using the MacTempas software package [15].

The images were calculated for an aberration-corrected FEI Titan 80–300 electron microscope operated at 300 kV accelerating voltage. Optical imaging parameters for an instrumental information limit close to 0.08 nm were applied in the image calculations [2,4,16]. Optimum negative phase contrast is obtained under these circumstances with a small negative spherical aberration of  $C_s = -15$   $\mu\text{m}$  in combination with a positive defocus of +6 nm, whereas optimum positive phase contrast is obtained with a positive spherical aberration of  $C_s = +15$   $\mu\text{m}$  and a negative defocus of –6 nm. It should be noted that the tuning of a negative spherical aberration for experimental HRTEM follows the same procedure as is used traditionally to apply a small positive spherical aberration, and does thus not require any additional expertise. In order to overcome the frequently reported Stobbs-factor problem [17], and to assure a quantitative match between the simulated and the experimental image contrast on an absolute scale, we considered the strong effect of the modulation transfer function (MTF) of the charge coupled device (CCD) camera on the image contrast [18]. Finally, the net effect of minor electronic and mechanical instabilities was additionally included in our simulations by an image convolution using a Gaussian vibration function with a  $1/e$  half-width of 0.03 nm.

A stochastic model was implemented in order to simulate the effect of fluctuating amorphous cover layers. The experimental observation shows that the contrast of these layers is fluctuating on the time scale of a single exposure, resulting in a noise-like contrast contribution to a single image. The effect of a single amorphous cover layer is represented in our simulations by a weak and random phase modulation of an initially plane electron wave, where the Fourier-space amplitude of the resulting wave

was subsequently adapted to the shape of the power spectrum of amorphous carbon. A set of stochastic images of amorphous cover layers was calculated for the optimized phase contrast conditions at negative and positive spherical aberration and added to the simulated images of the  $\text{SrTiO}_3$  crystal.

It is stated clearly that our simplified approach to add “amorphous” images to the perfect crystal images is only a semi-quantitative approximation. This approach neglects (i) the cross-diffraction between “amorphous” and crystalline intensity contributions inside the object and also (ii) the cross-interference between the respective wave function components during the electron-optical imaging process. However, a full dynamical calculation with a set of random atom configurations representing the amorphous material is beyond the scope of the present study. Due to the fact that the investigated diffraction scenario is still in the close-to-linear regime, and since the crystalline and the amorphous atom locations are spatially uncorrelated, the neglect of the resulting cross terms is of only minor relevance here, justifying the applied approximation.

Additional to the noise-like effect of the amorphous cover layers, the effect of electron shot noise was included in our simulations by assuming a dose of 200 electrons per CCD pixel. The electron dose was chosen quite high in the present case of a relatively radiation insensitive material, resulting in a comparatively small effect of the shot noise on the total image contrast.

## 3. Results

### 3.1. Image contrast and atom column intensity

Fig. 2 shows a thickness series of images calculated for the two alternative imaging modes. The displayed atom symbols clarify that the NCSI mode leads to a bright atom contrast under a darker background. This bright atom contrast is preserved up to an object thickness of  $t=7.7$  nm. In contrast, the traditional PCSI mode results in a dark atom contrast for relatively thin objects ( $t < 4.4$  nm), while bright peaks appear at the atom positions for an object thickness larger than 4.4 nm.

The difference in image contrast between the NCSI and the PCSI mode is already evident from the visual inspection of the two image series of Fig. 2. For a quantitative comparison, the images are normalized to a mean intensity of one, such that the standard deviation of the intensity reflects the image contrast. Fig. 3 displays the image contrast calculated for the two imaging scenarios as a function of the object thickness. The contrast resulting from the two alternative settings has essentially the same value at an object thickness of 1.1 nm. In the case of the NCSI mode the image contrast is strongly growing with increasing object thickness up to about 5.5 nm, where the contrast reaches a saturation value of about 0.27. The contrast increase of the PCSI mode with sample thickness is much smaller, and a saturation plateau occurs already in the thickness region between 3.3 and 7 nm. A further contrast increase in the PCSI mode near 7 and 8 nm is due to the appearance of a sharp intensity maximum in place of a previously shallow intensity minimum. For the thickness range of 3.3–6.6 nm, which is most suitable for high-performance HRTEM, the image contrast resulting from the NCSI mode is on average by about a factor of 2 larger than the related PCSI contrast.

A key requirement in quantitative HRTEM is the achievement of a good signal-to-noise ratio. The obtainable signal-to-noise ratio depends directly on the image intensity recorded at an atomic column and determines finally the precision of position and occupancy determinations. The image intensity values for the three types of columns, SrO, Ti, and O are plotted in Fig. 4 for the

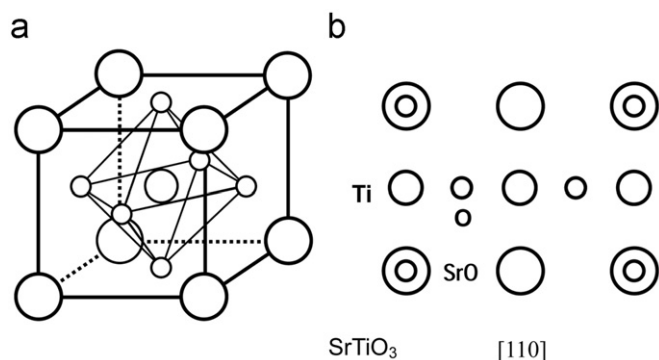
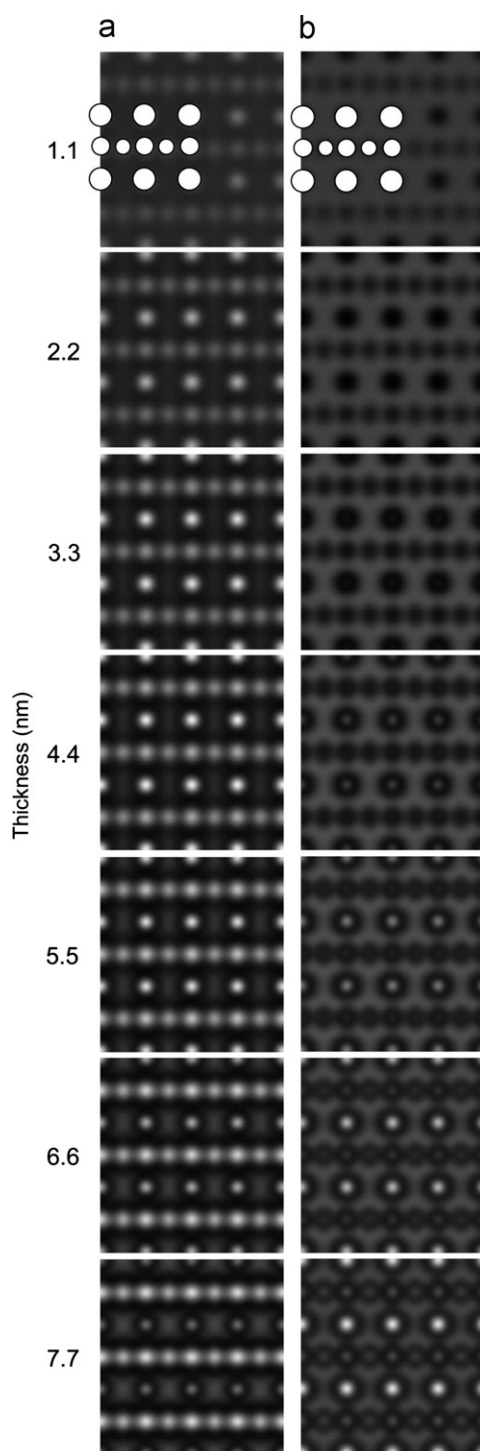
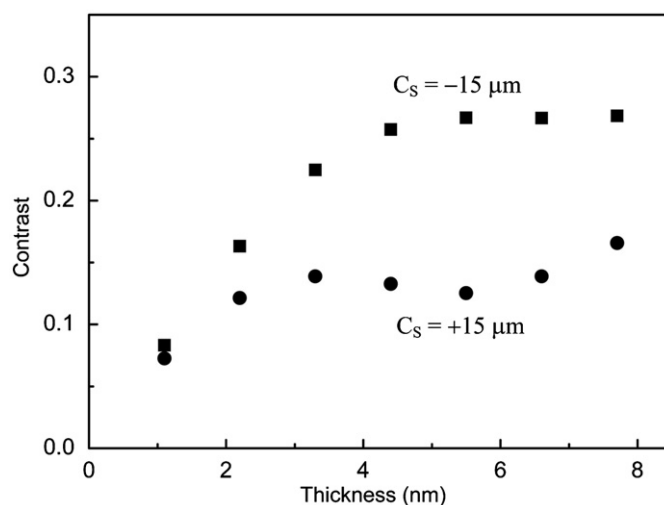


Fig. 1. Crystal structure of  $\text{SrTiO}_3$  in perspective view (a), and in view along the  $[110]$  direction (b).



**Fig. 2.** Thickness series of the  $[110]$  images of  $\text{SrTiO}_3$  calculated for (a) the NCSI mode with  $C_s = -15 \mu\text{m}$ , defocus of  $+6 \text{ nm}$ , and for (b) the PCSI mode with  $C_s = +15 \mu\text{m}$ , defocus of  $-6 \text{ nm}$ , assuming a microscope information limit of  $0.08 \text{ nm}$  and an accelerating voltage of  $300 \text{ kV}$ . The detector MTF, and additional instabilities described by a Gaussian distribution of image displacements with a  $1/e$  half-width of  $0.03 \text{ nm}$ , were taken into account. Positions of atomic columns are indicated in the insets at  $1.1 \text{ nm}$  object thickness.

images belonging to an object thickness of  $3.3 \text{ nm}$ . At this thickness, the positive  $C_s$  image reaches a local contrast maximum while the negative  $C_s$  image has a contrast which is still 20% lower than the saturation value reached at  $5.5 \text{ nm}$  object thickness. Fig. 4a shows the signal intensity associated with the SrO columns and Fig. 4b the signal intensity associated with the Ti



**Fig. 3.** Contrast under optimum imaging conditions as a function of sample thickness for the NCSI mode (squares) and for the PCSI mode (circles).

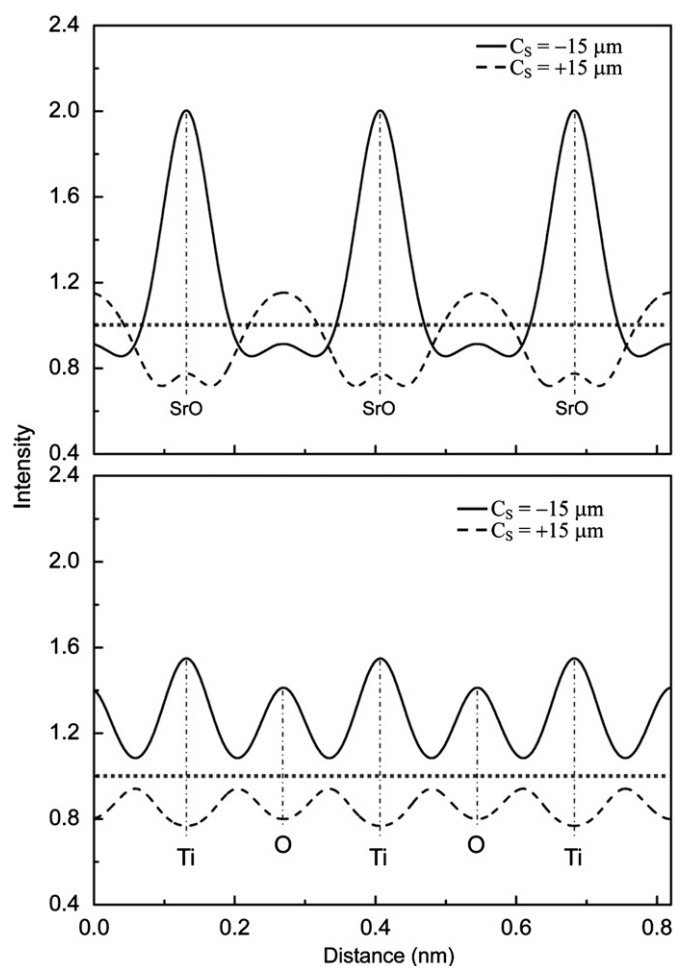


**Fig. 4.** Image intensity profiles belonging to SrO, Ti, and O columns with a thickness of  $3.3 \text{ nm}$  resulting from the NCSI mode (solid lines) and from the PCSI mode (dashed lines). Images are normalized to a mean value of 1.

and O columns. The solid-line profiles are taken from the images calculated for the NCSI mode and the dashed-line profiles are taken from the images calculated for the PCSI mode. The mean intensity  $I_{\text{mean}} = 1$  is denoted by a dotted line. The intensity

maxima  $I_{\max}$  ( $> 1$ ) of the solid-line profiles reflect the bright contrast at atomic column positions resulting from the NCSI mode. The intensity minima  $I_{\min}$  ( $< 1$ ) of the dashed-line profiles reflect the dark atom contrast obtained with the PCSI mode. For a quantitative comparison, the ratio of the column-based signal strength between the two imaging modes is defined by the ratio of the respective intensity extrema at column positions, given by  $(I_{\max} - I_{\text{mean}})_{\text{NCSI}} / (I_{\text{mean}} - I_{\min})_{\text{PCSI}}$ . The calculated results are 3.6 for SrO, 2.4 for Ti, and 2.1 for O. These ratios of the extremal values between the NCSI and the PCSI modes are for all individual column types even larger than the corresponding ratio of the overall image contrast of 1.6, which reflects the much stronger focused shape of the atomic columns in the NCSI mode.

Fig. 5 shows the dependence of the image intensity on the atomic number accumulated per individual atomic column along the viewing direction. It is noted that along the  $[1\ 1\ 0]$  direction a unit cell period of  $\text{SrTiO}_3$  includes two oxygen atoms in the oxygen column, one Ti atom in the Ti column, and one Sr atom plus one oxygen atom in the SrO column. The atomic numbers accumulated over a single unit cell period are thus 16 ( $2 \times 8$ ),

22, and 46 ( $8+38$ ) for the fully occupied oxygen column, the Ti column, and the SrO column, respectively. For the NCSI mode, the image intensity of all columns follows essentially a linear dependence on the total atomic number accumulated up to a thickness of at least 3.3 nm. Beyond this thickness the linear relation is still valid for the lighter Ti- and O-columns, whereas the linearity is lost for the heavier SrO columns due to the shorter extinction length of the latter column type. In the case of the PCSI mode, the linearity between column intensity and the accumulated atomic number is already lost for all column types at a thickness of 3.3 nm. Most importantly, the linear dependence of the column intensity on the accumulated atomic number exhibits also a higher slope in the NCSI mode than in PCSI mode.

### 3.2. Precision of atom-column position measurements

The  $\text{SrTiO}_3$  images of Fig. 2, which were simulated for a crystal thickness of 3.3 nm, were selected for investigating the effect of an amorphous layer on the measurement precision. In order to evaluate the effect of different amorphous layer thicknesses, one up to five random phase object images were added to the selected images of the  $\text{SrTiO}_3$  crystal as is illustrated in Fig. 6. The contrast scaling is identical for all displayed images. Since the intensity maxima produced by the NCSI mode are more pronounced in height and sharpness than the shallow intensity minima obtained with the PCSI mode, a comparatively stronger robustness of the atom column signal against noise can be expected for the NCSI mode. The superior signal-to-noise ratio of the NCSI mode should lead consequently also to a higher precision in the determination of atom column positions.

For each thickness of the amorphous layer the precision of the position measurement was quantified by a peak optimization procedure applied to 192 columns of SrO, Ti, and O, from a set of 64 stochastically modelled images. The resulting precision of the column position determination is shown in Fig. 7 as a function of the number of amorphous layers. The displayed precision values represent twice the standard deviation of the scatter in the peak position of a Gaussian peak profile after a non-linear least squares fit [14]. Overall, the precision obtained for the NCSI mode is by a factor of 2–3 better than the results of the PCSI mode. For the NCSI mode a precision well below 10 pm is easily obtained even for light-element columns and for comparably thick amorphous cover layers, whereas for the PCSI mode a much cleaner sample surface is definitely required in order to achieve the same level of precision. Most remarkably, for the same thickness of amorphous cover layers the measurement precision for the positions of the light-element O columns with the NCSI mode is as good as that for the heavy-element SrO columns with the PCSI mode.

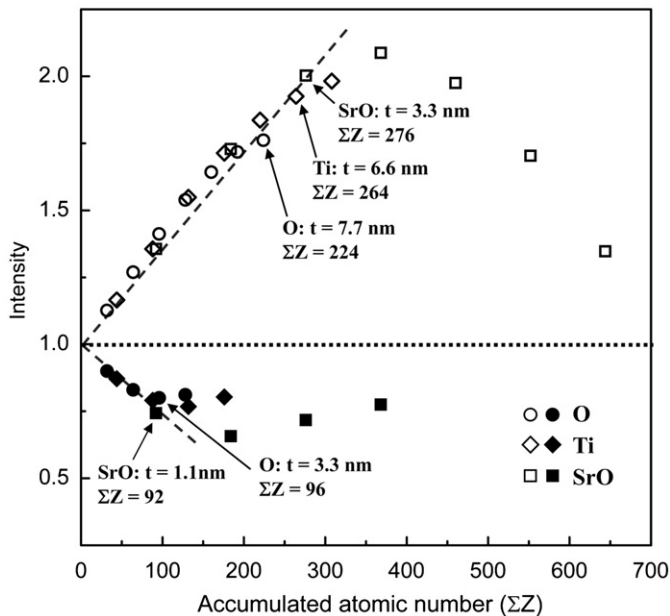


**Fig. 5.** Image intensity as a function of the accumulated atomic number  $\Sigma Z$  in atomic columns for the NCSI mode (open symbols, data  $>$  mean), and for the PCSI mode (solid symbols, data  $<$  mean). Object thickness values  $t$  belonging to the different column types are exemplarily noted.

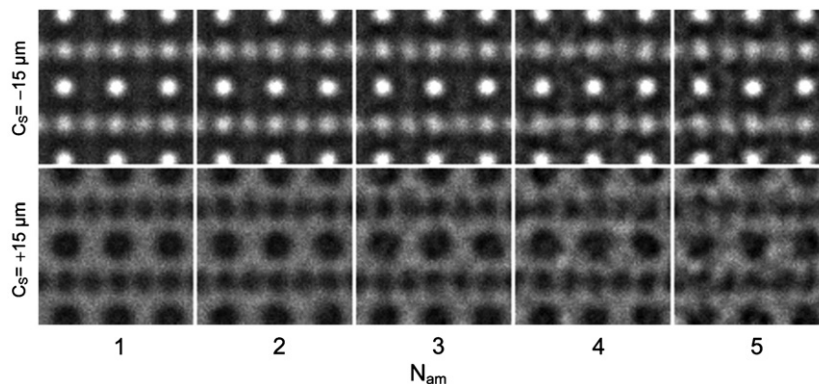


**Fig. 6.** Modelling of amorphous cover layers. The figure shows a particular set of simulated images of a  $\text{SrTiO}_3$  crystal with a thickness of 3.3 nm and various thicknesses of fluctuating amorphous cover layers. The thickness of the amorphous cover layers is given as the number  $N_{\text{am}}$  of random phase object images added to the crystal image.



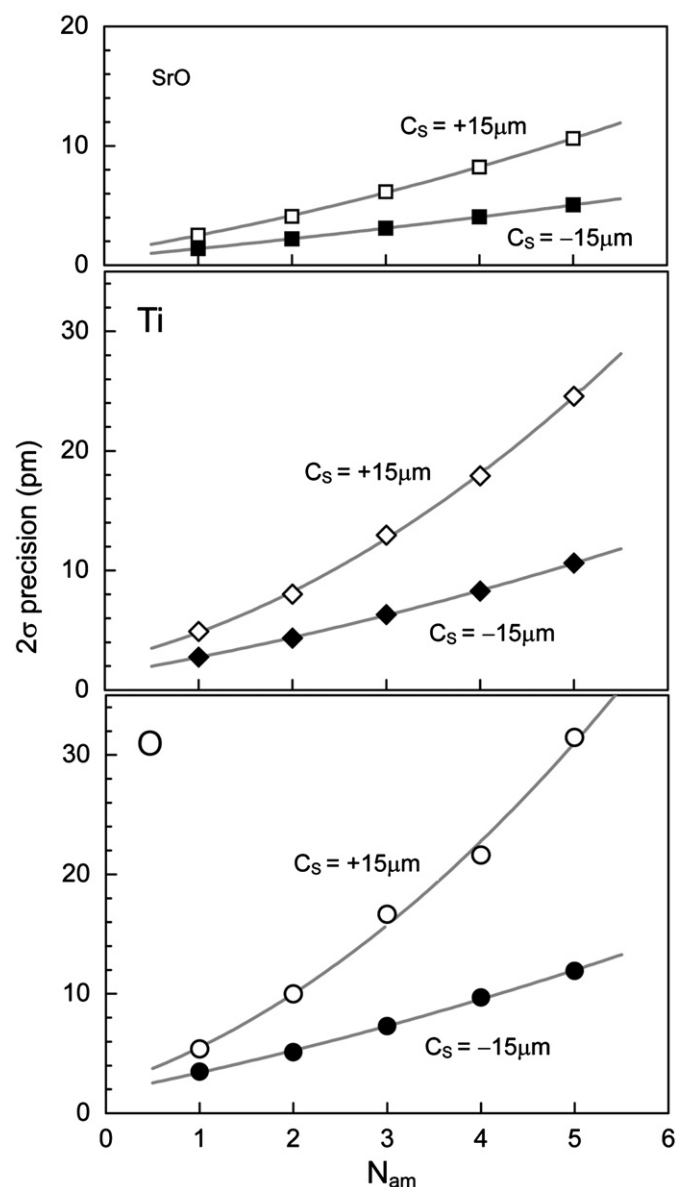


**Fig. 7.** Measurement precision for the position of SrO, Ti, and O atomic columns obtained with the PCSI mode (open symbols) and with the NCSI mode (solid symbols). The precision is given as twice the standard deviation ( $2\sigma$ ) of the scatter of the measured image peak positions. Each data point corresponds to the repeated measurement on a set of images of 3.3 nm thick  $\text{SrTiO}_3$  [110] with stochastically modelled amorphous cover layers. The number  $N_{am}$  of random phase object images used to simulate the effect of amorphous cover layers is proportional to the thickness of these layers.

#### 4. Discussion

The images obtained by applying the NCSI mode exhibit extraordinary advantages with respect to (i) the overall image contrast, (ii) the atom column intensity, and (iii) the linear dependence of the column intensity on the atomic number. The special features of the negative  $C_s$  images are a consequence of the reinforcement of the image contrast due to the constructive superposition of linear and non-linear contrast contributions in the case of thin objects [4–6]. We emphasize that our study is based on image simulations which match very closely realistic experimental conditions. The strong damping effect of the detector MTF on the image contrast was rigorously considered in our calculations together with the comparatively minor damping effect of electric and mechanical instabilities in order

to enable a quantitative match between the simulated and the experimental images on an absolute contrast scale. The difference in the contrast between the NCSI and the PCSI mode reported here would be even much stronger when disregarding the strong damping effect of the detector MTF. This is because of the fact that the MTF acts stronger on the sharp maxima generated by the NCSI mode than on the wider minima generated by the PCSI mode. An even stronger contrast difference between the two discussed imaging modes has thus to be expected in experiment with the future development of improved electron detectors.

In addition to a facilitated qualitative interpretation of atomic details, the enhanced image contrast with a negative  $C_s$  value provides also a reliable basis for a quantitative analysis of object structure details with superior sensitivity and robustness. The achievable precision for the measurement of atomic positions is by a factor of 2 up to 3 better when comparing the NCSI mode and the PCSI mode at an equal level of noise. The advantage of the NCSI technique with respect to precision even increases with the noise level. This is an important issue because the requirement for very clean specimen surfaces is not always fulfilled in experiment, and therefore image noise is an inevitable source of unsystematic errors in quantitative HRTEM. Furthermore, a strong dependence of the image intensity on the accumulated atomic number is highly advantageous for an accurate determination of the sample thickness and of chemical deviations from the perfect stoichiometry within compound materials. For the investigated case of perovskite materials, these requirements are certainly met for realistically thin specimens when applying the NCSI mode, while it is questionable if a comparable quality of structure investigations could be achieved with the traditional PCSI mode.

When quantifying atom column positions or their chemical composition, systematic errors need to be considered as well. Possible sources of systematic quantification errors are residual lens aberrations, a local change of sample thickness, and small unavoidable tilts of the specimen orientation away from the fully symmetric Laue orientation. These error sources are usually taken into account by carrying out an iterative procedure in which an experimental image is compared to simulated images following established procedures [8,19–22]. Owing to the superior sensitivity and linearity of the atom column signal in negative  $C_s$  images, systematic quantification errors can be reduced more reliably since model-based calculated images can be matched more accurately to experimental images.

#### 5. Conclusion

The NCSI mode in aberration-corrected electron microscopy offers unique advantages for direct atomic imaging in HRTEM. In the case of thin objects the NCSI mode is clearly superior to the traditional PCSI mode due to its characteristic strong contrast. The strong contrast provided by the NCSI mode is highly sensitive to the atomic number accumulated along atomic columns, allowing to determine stoichiometric variations with unprecedented precision in combination with image calculations. The NCSI mode is therefore particularly useful for studying compound materials including lower nuclear charge elements, such as oxygen in perovskites. Furthermore, the strong contrast offered by the NCSI mode provides also a reliable noise-resistant basis for a highly accurate quantification of atom positions, enabling a precision in the picometer range.

#### Acknowledgment

The authors are grateful to K. Tillmann and K. Urban for valuable discussions.

## References

- [1] M. Haider, S. Uhlemann, E. Schwan, H. Rose, B. Kabius, K. Urban, *Nature* 392 (1998) 768.
- [2] M. Lentzen, B. Jahnen, C.L. Jia, A. Thust, K. Tillmann, K. Urban, *Ultramicroscopy* 92 (2002) 233.
- [3] C.L. Jia, M. Lentzen, K. Urban, *Science* 299 (2003) 870.
- [4] C.L. Jia, M. Lentzen, K. Urban, *Microsc. Microanal.* 10 (2004) 174.
- [5] M. Lentzen, *Ultramicroscopy* 99 (2004) 211.
- [6] K. Urban, C.L. Jia, L. Houben, M. Lentzen, S.B. Mi, K. Tillmann, *Philos. Trans. R. Soc. A* 367 (2009) 3735.
- [7] C.L. Jia, K. Urban, *Science* 303 (2004) 2001.
- [8] C.L. Jia, S.B. Mi, K. Urban, I. Vrejoiu, M. Alexe, D. Hesse, *Nat. Mater.* 7 (2008) 57.
- [9] C.L. Jia, S.B. Mi, K. Urban, I. Vrejoiu, M. Alexe, D. Hesse, *Phys. Rev. Lett.* 102 (2009) 117601.
- [10] C.L. Jia, S.B. Mi, M. Faley, U. Poppe, J. Schubert, K. Urban, *Phys. Rev. B* 79 (2009) 081405.
- [11] A.J. Den Dekker, J. Sijbers, D. Van Dyck, *J. Microsc.* 194 (1999) 95.
- [12] A.J. Den Dekker, S. Van Aert, A. van den Bos, D. Van Dyck, *Ultramicroscopy* 104 (2005) 83.
- [13] S. Van Aert, A.J. Den Dekker, A. van den Bos, D. Van Dyck, J.H. Chen, *Ultramicroscopy* 104 (2005) 107.
- [14] L. Houben, A. Thust, K. Urban, *Ultramicroscopy* 106 (2006) 200.
- [15] M.A. O'Keefe, R. Kilaas, *Scan. Microsc. Suppl.* 2 (1988) 225.
- [16] J. Barthel, A. Thust, *Phys. Rev. Lett.* 101 (2008) 200801.
- [17] M.J. Hytch, W.M. Stobbs, *Ultramicroscopy* 53 (1994) 191.
- [18] A. Thust, *Phys. Rev. Lett.* 102 (2009) 220801.
- [19] A. Thust, K. Urban, *Ultramicroscopy* 45 (1992) 23.
- [20] G. Möbus, M. Rühle, *Ultramicroscopy* 56 (1994) 54.
- [21] W.E. King, G.H. Campbell, *Ultramicroscopy* 56 (1994) 46.
- [22] K. Urban, *Science* 321 (2008) 506.